Atmospheric
Chemistry
and Physics
Open Access
Discussions

Measurements of dust deposition velocity in a wind-tunnel experiment

J. Zhang[1,2]**, Y. Shao**[2]**, and N. Huang**[1]

[1]Key Laboratory of Mechanics on Disaster and Environment in Western China, Lanzhou University, 730000 Lanzhou, China
[2]The Institute for Geophysics and Meteorology, University of Cologne, 50973 Cologne, Germany

Correspondence to: J. Zhang (zhang-j@lzu.edu.cn)

Discussion Paper | Discussion Paper | Discussion Paper | Discussion Paper

ACPD

14, 9439–9474, 2014

Measurements of dust deposition velocity

J. Zhang et al.

Title Page

Abstract	Introduction
Conclusions	References
Tables	Figures

|◄ | ►|
◄ | ►

Back | Close

Full Screen / Esc

Printer-friendly Version

Interactive Discussion

Abstract

In this study, we present the results of a wind-tunnel experiment on dust deposition. A new method is proposed to derive dust deposition velocity from the PDA (Particle Dynamics Analysis) particle-velocity and particle-size measurements. This method has the advantage that the motions of individual dust particles are directly observed and all relevant data for computing dust deposition velocity is collected using a single instrument, and therefore the measurement uncertainties are reduced. The method is used in the wind-tunnel experiment to measure the dust deposition velocities for different particle sizes, wind speeds and surface conditions. For a sticky-smooth wood surface and a water surface, the observed dust deposition velocities are compared with the predictions using a dust deposition scheme, and the entire dataset is compared with the data found in the literature. From the wind-tunnel experiments, a relatively reliable dataset of dust deposition velocity is obtained, which is of considerable value for the development and validation of dust deposition schemes.

1 Introduction

In the past few decades, the dust research community has been struggling to develop dust emission and deposition schemes for large scale dust models. As far as dust emission is concerned, several wind-tunnel and field observations have been carried out (e.g. Gillette, 1976; Shao et al., 1993; Sow et al., 2006; Ishizuka et al., 2008) which serve as the basis for the conceptualization of the dust emission schemes (Shao, 2001, 2004; Marticorina and Bergamatti, 1995; Alfaro and Gomes, 2001). The understanding of dust deposition is at least as poor as that of dust emission (Goossens and Offer, 2000). The samplers used for dust-deposition measurements in field experiments have been found to be quite inefficient (Sow et al., 2006). The large uncertainties in the dust-deposition estimates in regional and global dust models have been documented by Uno et al. (2006) and Textor et al. (2006, 2007). Our preliminary test of the dust

deposition schemes shows that the scheme estimates can easily differ by an order of magnitude, and it is often unclear how the scheme parameters should be specified in regional and global dust models.

We must come to terms with several problems in dust-deposition parameterizations,
5 but the most outstanding is the serious lack of high-quality and cohesive datasets for testing dust-deposition theories and schemes. Field observations on dust deposition over time intervals of days and weeks have been made using direct or indirect techniques (e.g. Gao et al., 1997; Liu et al., 2004). Such observations are valuable in determining the order of magnitude of dust deposition for given areas, but do not provide
10 sufficient details for the conceptualization and derivation of dust-deposition theories. Chamberlain (1967) conducted a wind-tunnel experiment on the deposition of particles of various sizes over a surface of artificial sticky grass. His data have proved to be very useful for the verification of dust-deposition schemes. However, natural surfaces are very different from a sticky grass surface in physical and aerodynamic characteristics.
15 Only very few surface types have been investigated in wind-tunnel studies so far, and to our knowledge no equivalent field experiments have ever been carried out.

Dust deposition is mostly parameterized through deposition velocity, w_d, and in most dust-deposition experimental studies, measurements of dust flux and/or concentration are made for the estimation of w_d (Sehmel, 1971; Wesley et al., 1983; Gallagher et al.,
20 1997; Ould-Data, 2002; Pryor et al., 2008). Various techniques and devices have been used (Seinfeld and Pandis, 1998) and measurements made under different conditions. As a consequence, the comparability between the datasets has been poor (Wesely et al., 1985; Hicks et al., 1989; Goossens and Rajot, 2008). As shown in Fig. 1, a large scatter over orders of magnitude among the measurements published in the litera-
25 ture exist. Such scatter seriously undermines the value of the measurements for the validation of models, which may be partly attributed to the uncertainty in measuring techniques and differences in the experimental conditions. A considerable discrepancy between the measurements and the model estimates is also apparent, due to reasons which are yet to be fully explained.

In this paper, we propose a new method for directly measuring dust deposition velocity use a single device, a Particle Dynamics Analysis (PDA). This technique has the advantage of observing the motion of individual particles and avoids uncertainties arising from using a combination of devices. Wind-tunnel experiments are carried out
5 by using the PDA to measure dust deposition velocities for various surfaces, ranging from a sticky-smooth wood surface (wood surface hereafter) to a rough vegetation surface, and a reliable dataset is obtained. The measurements are then used to test the Slinn and Slinn (1980, SS80 hereafter) scheme for smooth (wood and water) surfaces. The advantages of our technique are demonstrated and the possible improvements
10 required in the SS80 scheme are identified. The dust deposition velocities measured in our experiments are compared with those of several other experiments published in the literature after correction of all data to the same reference height (1 m).

2   Particle Dynamics Analysis (PDA) and wind-tunnel experiment

PDA is an extension of the LDA (Laser Doppler Anemometry), which can measure
15 both the velocity and size of a particle passing through the measuring point. Particle velocity is measured by using the laser Doppler Effect and particle size the phase shift between the two signals of the scattered light from two detectors in the receiver (Dantec Dynamics A/S, 2006).

Figure 2 illustrates the functioning principle of the PDA. A laser beam emitted from
20 the generator is split into two coherent beams. These beams intersect to form a measuring point with an elliptical volume and the interference produces parallel bright and dark planes, known as fringes. The distances between the fringes depend on the laser wavelength and the angle between the incident beams (upper right corner of Fig. 2). When a particle moves cross the fringes, a current pulse (right hand of Fig. 2) will be
25 generated by the photo-detector because of the changing intensity of the light scattered by the particle, which alternates between the bright and dark fringes. For the time interval between the peaks of the pulses can be obtained and the particle displacement

(in the direction perpendicular to the fringes) is the spacing of the adjacent fringes, the velocity component orthogonal to the fringes can be determined. This is the so called "fringes model" of the PDA. Also, an aperture plate as shown in the lower right corner of Fig. 2 is used as a multi-light detector, and the phase shift between the Doppler signals from the different detectors can be obtained to deduce the size of the passing particle.

The structure of the Lanzhou University (LZU) wind tunnel is shown in Fig. 3. It is a blow-down wind tunnel of 55 m long, including a fan, a rectification section, a working section and a diffuser. High-speed and turbulent wind can be generated by the fan of 75 kW. The turbulent air flows into the rectification section where the flow speed slows down because of the bigger cross-section. Turbulent eddies in the original flow generated by the fan are destructed by a combination of honeycomb and damping screens (rectangular grids) deployed in this part. After passing the rectification section, the air flow becomes uniform. The rectified air flow is accelerated in the working section which has a smaller but uniform cross-section of 1.3 m × 1.45 m ($w \times h$). The length of the working section is about 22 m. Some spires or roughness elements (or both) are set up in the front of this section to generate a turbulent boundary layer. Finally, the air flows out from the diffuser with an increasing cross-section. The wind tunnel is controlled by a computer and the wind speed can be adjusted between 3 and 40 m s^{-1}.

The configuration of the wind-tunnel experiment is as shown in Fig. 4. A six-meter long roughness-element section is located in the front of the working section to generate a deep turbulent boundary layer. Downstream of this section is the test surface. A dust feeder is placed at the beginning of the working section to inject dust into the tunnel through a tubular manifold which consists of two rows of six outlets with even spacing of 0.2 m (Fig. 4a). The manifold is adjusted such that the bottom and the top rows are at approximately 0.2 m and 0.4 m above the top of the surface. After release, the dust particles are fully dispersed in the turbulent boundary layer over the test surface. The PDA is located near the end of the working section and the distance between the measuring point and the dust outlet is about 10 m to ensure sufficient development

of the turbulent boundary layer and dust dispersion. The height of the measuring point is fixed as close to the surface as possible (Fig. 4c).

The PDA works best for spherical particles. Therefore, the optical characteristics and spherical degree of the particles are important factors which affect the reliability of the PDA measurements. A white powder of Silicon Dioxide (SiO_2) with density of $2200\,kg\,m^{-3}$ is selected as the dust source for our experiments. These particles have a good spherical degree and the mean diameter is $10\,\mu m$ (Fig. 5).

Dust deposition over different surfaces is investigated in our wind-tunnel experiments, including a wood and a water surface, which we will discuss later in detail. For both surfaces, particle rebound is not possible and thus it is reasonable to assume that dust concentration at the surface is zero, an important assumption made in most dust deposition schemes. For these reasons, dust deposition over the wood and water surfaces is relatively simple and suitable for testing the PDA technique against theory and for examining the essence of dust deposition parameterizations. The experiments are then operated over sand, sandy loam, Gobi and tree surfaces to produce a more complete dataset.

The experimental procedure is as follows:

1. *Preparation:* the instruments are arranged as shown in Fig. 4. In case of the wood surface, lubricating oil is applied to floor to make it sticky. The sand and sandy loam surfaces are wetted and then air dried to produce a crust to prevent emission of surface particles.

2. *Profile Measurement*: about 10 points of different heights are selected. Dust particles are released from the feeder and the speeds of the dust particles passing through the points are measured using the PDA. As the particles are small, their horizontal velocities can be considered to be the same as the wind speed. At each point, the horizontal particle velocities and concentrations are measured and then averaged over 3 min intervals, to produce the mean wind and dust concentration profiles.

3. *Point Measurement*: a point, at about 15 mm above the surface, is selected for dust deposition measurement. The velocities and sizes of the particles that pass through this point are measured with the PDA. The duration of the measurement is 10 min.

4. *Repeat*: the surface is re-prepared and the Steps 2 and 3 are repeated.

The experiments are carried out for different wind speeds and for each wind speed at least 3 successful runs are made. For the PDA can only identify particles bigger than 0.5 µm (limited by the wavelength of the laser beam), the raw data are divided into the following of particle size bins, 0.5, 1.5, 3, 5, 10, 15, 20, 25, 30, 50, 80, 100, 150 and 200 µm. For each bin, the particles are considered to be mono-dispersed with the respective median sizes of 1, 2.25, 4, 7.5, 12.5, 17.5, 22.5, 27.5, 40, 65, 90, 125 and 175 µm. The deposition velocity for each size bin is obtained by using the technique described in Sect. 3.

3 Methodology of PDA data processing

We now describe the method for deriving dust deposition velocity for different particle-size bins based on the PDA measurements. Our discussion is confined to the vertical direction. As shown in Fig. 6, the sampling area of the PDA has a volume of V. If no particle appears in V, then dust concentration in it is zero. If particle i of mass m_i passes through V with (vertical) velocity w_{pi} then the corresponding concentration over the transit time Δt_i is m_i/V and the associated dust flux is

$$F_i = \frac{m_i}{V} \cdot w_{pi} \tag{1}$$

Suppose the sampling time interval is T, during which N particles pass through V. Then, the average dust concentration c and dust flux F_d are respectively

$$c = \sum_{i=1}^{N} \left(\frac{m_i}{V} \cdot \frac{\Delta t_i}{T} \right) \qquad (2)$$

$$F_d = \sum_{i=1}^{N} \left(\frac{m_i}{V} \cdot w_{pi} \cdot \frac{\Delta t_i}{T} \right) \qquad (3)$$

The deposition velocity can be expressed by combining Eqs. (2) and (3) as

$$w_d = \frac{\sum_{i=1}^{N} \left(D_{pi}^3 \cdot w_{pi} \cdot \Delta t_i \right)}{\sum_{i=1}^{N} \left(D_{pi}^3 \cdot \Delta t_i \right)} \qquad (4)$$

where D_{pi} (particle diameter), w_{pi} and Δt_i are measured simultaneously by the PDA.

The deposition velocity calculated with Eq. (4) includes the contributions of Brownian diffusion, eddy diffusion, gravitational settling and is possibly affected by the mean vertical wind $\overline{w}_a$. While $\overline{w}_a$ is generally considered to be zero, in our wind-tunnel experiments, it may be locally of the order of magnitude comparable to the particle terminal velocity. Even if it is zero in reality, error in flow measurements may still occur because a small alignment error in the PDA vertical with respect to the surface normal may result in interpreting a component of the horizontal wind as the vertical wind and cause a serious bias in the deposition velocity estimates. Therefore, we must remove the effect of $\overline{w}_a$ from Eq. (4).

Our approach is to first remove the mean particle (vertical) motion ($\overline{w}_p$) from w_d, which is composed of the mean air (vertical) motion ($\overline{w}_a$) and gravitational settling terminal velocity w_t, i.e., $\overline{w}_p = \overline{w}_a + w_t$, then to add w_t back to w_d. Equation (4) can now

be written as

$$w_d = \frac{\sum_{i=1}^{N} \left(D_{pi}^3 \cdot w_{pi} \cdot \Delta t_i \right)}{\sum_{i=1}^{N} \left(D_{pi}^3 \cdot \Delta t_i \right)} - \overline{w}_p + w_t \qquad (5)$$

where w_t is computed with

$$w_t = \frac{C_c \rho_p D_p^2}{18\mu} \cdot g \qquad (6)$$

with C_c being the Cunningham correction factor, D_p the mean particle diameter of the particle-size bin, μ dynamic air viscosity, ρ_p the particle density and g the gravitational acceleration. However, the calculation of $\overline{w}_p$ from the PDA particle-velocity measurements requires a correction of sampling bias. Particles observed by the PDA can be considered to be discrete samplers of the flow speed. Due to the uneven particle-number distribution with height (e.g. more particles moving downward than upward), the sampling of w_p may be biased, as shown in Fig. 7. In that figure, the dots represent w_p measured by the PDA, and the solid line $w_a + w_t$. The upward air motion is less frequently observed by the PDA due to the lower dust concentration at smaller height. The situation is the opposite for the downward air motion. To estimate $\overline{w}_p$ (bold dashed line in Fig. 7), the full dataset of w_p is initially divided into two subsets according to its sign, and $\overline{w}_p$ set to $(\overline{w}_p^+ + \overline{w}_p^-)/2$, with $\overline{w}_p^+$ and $\overline{w}_p^-$ being respectively the mean values of the positive and negative particle velocities. The full dataset is then divided into four subsets as follows

(1) $w_p \in (0, \overline{w}_p)$;

(2) $w_p \in (\overline{w}_p, 2\overline{w}_p)$;

(3) $w_p > 2\overline{w}_p$, if $\overline{w}_p > 0$ (or $w_p < 2\overline{w}_p$, if $\overline{w}_p < 0$); and

(4) $w_p < 0$, if $\overline{w}_p > 0$ (or $w_p > 0$, if $\overline{w}_p < 0$).

The number of measurements of subset j, N_j, is counted, and the average of particle velocity deviation of the subset $\overline{w_p - \overline{w}_p}^{N_j}$ is calculated. As an example for $\overline{w}_p > 0$ (corresponding to Fig. 7), $\overline{w}_p$ is determined iteratively to satisfy

$$\overline{w_p - \overline{w}_p}^{N_2} \cdot \frac{N_2}{N_2 + N_3} + \overline{w_p - \overline{w}_p}^{N_3} \cdot \frac{N_3}{N_2 + N_3} = \overline{w_p - \overline{w}_p}^{N_1} \cdot \frac{N_2}{N_2 + N_3} + \overline{w_p - \overline{w}_p}^{N_4} \cdot \frac{N_3}{N_2 + N_3} \quad (7)$$

4 Results

Figure 8 shows two examples of the six surfaces tested in the experiments. For each surface, the experiment is repeated under three wind conditions. As an example, the wind profiles over the water surface are shown in Fig. 9. The logarithmical wind profile

$$u_a(z) = (u_*/\kappa) \cdot \ln[(z - z_d)/z_0] \quad (8)$$

is fitted to the data for the estimates of the friction velocity, u_*, and roughness length, z_0. The zero-plane displacement height, z_d, is set to zero for the low-roughness surfaces (wood, water, sand, loam and Gobi), but to 200 mm for the tree surface. κ is von Karman constant (~ 0.4).

Figure 10 shows the observed deposition velocity for the wood surface, which increases as expected with friction velocity. The SS80 scheme (Appendix A) is originally proposed for water surfaces, but is applicable to other smooth surfaces if the particle-growth mechanism embedded in the scheme is excluded. The predictions of the SS80 scheme are also shown in Fig. 10, which are generally comparable with, the measurements although somewhat smaller. The underestimation by the scheme can be attributed to the inaccurate estimates of the dust transfer through the laminar layer. For very small particles (about 1 μm) under high friction velocity, the observed w_d

showed occasional negative values (lower right corner of Fig. 10), probably due to the re-suspension of the deposited particles.

Water surface is special because it is wet and sticky. The air layer of high humidity adjacent to the water surface promotes the growth of hygroscopic particles and thereby enhances their gravitational settling. The SS80 scheme was proposed for parameter-izing dust deposition to water surfaces by accounting for this mechanism. However, the dust particles used in our study are hydrophobic and thus the enhanced gravita-tional settling due to particle-size growth must be excluded from the SS80 scheme. Compared with the observation, the SS80 scheme is found to substantially underes-timate dust deposition velocity (not shown). The failure of the SS80 scheme is most probably due to the neglect of another important mechanism, that it, under windy con-ditions, dust deposition to the water surface can be significantly enhanced by waves and spray droplets. The effects of waves and spray droplets are included in the SS80 scheme, but can be accounted for by reducing the laminar layer resistance to zero. The predicted dust deposition velocities using the modified SS80 scheme by setting the laminar-layer resistance to zero are now found to agree much better with the mea-surements as shown in Fig. 11. It is also observed that w_d increases almost linearly with friction velocity, and for particles in the size range of $0.5\,\mu m < D_p < 10\,\mu m$, w_p is almost constant (particle-size independent) for given wind speed. This is caused by the indistinctive collection of particles with different sizes by waves and spray droplets.

The above described techniques of wind-tunnel experiment and data analysis are also applied to sand, sandy loam, Gobi and tree surfaces. A relatively comprehensive dataset of dust deposition for different surfaces, particle sizes and wind conditions is obtained, as shown in Fig. 12. Some negative deposition velocities were occasionally observed, possibly due to the additional dust emission from the surface. Although we took measures to reduce dust re-suspension and unwanted dust emission, by oiling the surface or promoting crust formation prior to the experiment, it was not possible to entirely suppress the re-suspension of the dust deposited to the surface and dust emission from the surfaces when crust was destructed by wind and turbulence during

the experiments. Also over the tree surface, occasional negative deposition velocities were observed. This may be caused by measurement errors in case of low dust concentrations for some particle-size bins, which result in inaccurate estimates of $\overline{w}_p$ and hence w_d.

5   The sand, sandy-loam, Gobi and tree surfaces are relatively rough surfaces. We have tested the SS80 and the Slinn (1982) scheme against our data, but good agreements between the model predictions and the measurements cannot be achieved by setting the scheme parameters in reasonable ranges. A new scheme needs to be developed to overcome the deficiencies in the existing scheme in parameterizing dust deposition
10   over rough surfaces, which we will discuss in detail in a companion paper.

It is appropriate to put our dataset in perspective to the existing data published in the literature. However, dust deposition velocity is dependent on the reference height, z_r, at which dust concentration is also measured to compute dust deposition flux. In our wind-tunnel experiments, z_r was set to 15 mm above the tunnel floor, while various
15   reference heights were used in the other existing studies. To facilitate comparison, we have therefore corrected all data to the same reference height (1 m) using the following equation

$$w_{dc} = \left\{ \left[\frac{1}{w_d(z)} - \frac{1}{w_t} \right] \left(\frac{z - z_d}{z_r - z_d} \right)^{\frac{w_t}{\kappa u_*}} + \frac{1}{w_t} \right\}^{-1} \tag{9}$$

where w_{dc} is the deposition velocity at z_r and z height of the measuring point. Figure 13
20   shows the comparison between our data with the existing data of dust deposition velocity. As seen, our data are in general consistent with the existing studies.

5   Summary

We carried out wind-tunnel experiments to measure dust deposition velocity for different particle sizes, surfaces and wind velocities. A new method based on the PDA

technique was proposed for the measurements. This technique is more reliable than other dust deposition measuring techniques, as it directly measures the motion of the dust particles. The PDA method was first applied to a sticky-smooth wood surface and a water surface and the measurements compared with the SS80 scheme predictions.

5 For these surfaces, the SS80 scheme is expected work reasonably well. For the wood surface, good agreement between the measurements and the scheme predictions was found, and for the water surface, the measurements and the scheme estimates only agree if the effect of waves and spray droplets on dust deposition is taken into consideration. These comparisons confirm the effectiveness of the method we proposed.

10 After testing the PDA method for the simple (wood and water) surfaces, the technique was then applied to measuring dust deposition over four other surfaces including sand, sandy loam, Gobi and vegetated (tree) surfaces. A reliable dataset of dust deposition velocity for six surface types, three velocities and 9 particle size groups (ranging from 0.5 to 40 µm) is obtained. This dataset is an enrichment of the existing dust deposition

15 data, has relatively high accuracy and serves as a reference for development of dust deposition schemes.

It is found that dust deposition velocity for particles in the 0.5–40 µm size range increases with particle size and friction velocity. In comparison with the other surfaces, the deposition velocity is large for the water surface (because of waves and spray

20 droplets) and the tree surface (because of efficient surface collection). We have used the measurements to test the performance of some existing schemes and have found that they generally perform poorly for rough surfaces. This finding suggests that better representation of surface roughness elements in dust deposition schemes is required. In a companion paper, we will propose a new dust deposition scheme and validate the

25 scheme with the observations from our wind-tunnel experiments.

Appendix A

The Scheme of Slinn and Slinn (1980) for dust deposition

Slinn and Slinn (1980) used a two-layer model (depicted in Fig. A1) to explain dust deposition over a water surface, which is considered to be smooth (without roughness elements) and wet (leading to hygroscopic growth of particle size). The atmosphere below a certain height is divided into two layers, an upper constant flux layer of depth z_r, where turbulent diffusion dominants, and a lower deposition layer of depth δ, where molecular diffusion dominants. Dust is transferred to the surface by impaction, Brownian diffusion and gravitational settling. The dust deposition velocity over the water surface is expressed as

$$\frac{1}{w_d} = \frac{1}{w_C} + \frac{1}{w_D} - \frac{w_t(D_p)}{w_C w_D}$$

where

$$w_C = \frac{1}{1-\kappa} \cdot \frac{u_*^2}{\overline{u}_a(z_r)} + w_t(D_p)$$

is the transfer velocity for the upper layer, with u_* being friction velocity, $\overline{u}_a(z_r)$ the mean wind speed at reference level z_r, κ the von Karman constant; $w_t(D_p)$ is the particle terminal velocity and

$$w_D = -\alpha m'' + \frac{1}{\kappa} \cdot \frac{u_*^2}{\overline{u}_a(z_r)} \cdot \left(Sc^{-1/2} + 10^{-3/\tau_p^+} \right) + w_t(D_{p,\,w})$$

is the transfer velocity for the low deposition layer, where m'' represents the contribution from diffusiophoresis and $\alpha = 10^3\,\mathrm{cm\,s^{-1}}/(1\,\mathrm{g\,cm^{-2}\,s^{-1}})$. Hygroscopic growth of particles is taken into account. D_p and $D_{p,\,w}$ represent the diameter of dry and wet particle, respectively. Here, both the Schmidt number (Sc) and the dimensionless relaxation time (τ_p^+) relates to the wet particle diameter.

Discussion Paper | Discussion Paper | Discussion Paper | Discussion Paper |

ACPD

14, 9439–9474, 2014

Measurements of dust deposition velocity

J. Zhang et al.

Title Page

Abstract | Introduction

Conclusions | References

Tables | Figures

|◀ | ▶|

◀ | ▶

Back | Close

Full Screen / Esc

Printer-friendly Version

Interactive Discussion

Appendix B

Dataset of the wind-tunnel experiment

See Tables B1 and B2.

References

Alfaro, S. C. and Gomes, L.: Modeling mineral aerosol production by wind erosion: emission intensities and aerosol size distributions in source areas, J. Geophys. Res., 106, 18075–18084, 2001.

Beswick, K. M., Hargreaves, K. J., Gallagher, M. W., Choularton, T. W., and Fowler, D.: Size-resolved measurements of cloud droplet deposition velocity to a forest canopy using an eddy correlation technique, Q. J. Roy. Meteor. Soc., 117, 623–645, 1991.

Bleyl, M.: Experimentelle Bestimmung der Depositionsgeschwindigkeit Luftgetragener Partikel mit Hilfe der Eddy-Kovarianzmethode über einem Fichtenaltbestand im Solling, Ph.D. thesis, Georg-August-Universität, Göttingen, 2001.

Chamberlain, A. C.: Transport of Lycopodium spores and other small particles to rough surfaces, P. Roy. Soc. Lond. A Mat., 296, 45–70, 1967.

Clough, W. S.: Transport of particles to surfaces, J. Aerosol Sci., 4, 227–234, 1973.

Clough, W. S.: The deposition of particles on moss and grass surfaces, Atmos. Environ., 9, 1113–1119, 1975.

Dantec Dynamics A/S: BSA Flow Software Installation and User's Guide, Version 4.10, Skovlunde, 2006.

Gallagher, M. W., Beswick, K. M., Duyzer, J., Westrate, H., Choularton, T. W., and Hummelshøj, P.: Measurements of aerosol fluxes to speulder forest using a micrometeorological technique, Atmos. Environ., 31, 359–373, 1988.

Gallagher, M. W., Beswick, K. M., Duyzer, J., Westrate, H., Choularton, T. W., and Hummelshøj, P.: Measurements of aerosol fluxes to speulder forest using a micrometeorological technique, Atmos. Environ., 31, 359–373, 1997.

Gao, Y., Arimoto, R., Duce, R. A., Zhang, X. Y., Zhang, G. Y., An, Z. S., Chen, L. Q., Zhou, M. Y., Gu, D. Y.: Temporal and spatial distributions of dust and its deposition to the China Sea, Tellus B, 49, 172–189, 1997.

Gillette, D. A.: Fine particulate emissions due to wind erosion, Paper (s)/American society of agricultural engineers.(Meetings.) 1976. No. 2018. St. Joseph: ASAE, 1976.

Ginoux, P., Prospero, J. M., Torres, O., and Chin, M.: Long-term simulation of global dust distribution with the GOCART model: correlation with North Atlantic Oscillation, Environ. Modell. Softw., 19, 113–128, 2004.

Goossens, D. and Offer, Z. Y.: Wind tunnel and field calibration of six aeolian dust samplers, Atmos. Environ., 34, 1043–1057, 2000.

Goossens, D. and Rajot, J. L.: Techniques to measure the dry aeolian deposition of dust in arid and semi-arid landscapes: a comparative study in West Niger, Earth Surf. Proc. Land., 33, 178–195, 2008.

Grönholm, T., Aalto, P. P., Hiltunen, V., Rannik, Ü., Rinne, J., Laakso, L., Hyvönen, S., Vesala, T., and Kulmala, M.: Measurements of aerosol particle dry deposition velocity using the relaxed eddy accumulation technique, Tellus B, 59, 381–386, 2007.

Hicks, B. B., Matt, D. R., McMillen, R. T., Womack, J. D., Wesely, M. L., Hart, R. L., Cook, D. R., Lindberg, S. E., de Pena, R. G., and Thomson, D. W.: A field investigation of sulfate fluxes to a deciduous forest, J. Geophys. Res., 94, 13003–13011, 1989.

Ishizuka, M., Mikami, M., Leys, J., Yamada, Y., Heidenreich, S., Shao, Y., and McTainsh, G. H.: Effects of soil moisture and dried raindroplet crust on saltation and dust emission, J. Geophys. Res., 113, D24212, doi:10.1029/2008JD009955, 2008.

Jickells, T. D., An, Z. S., Andersen, K. K., Baker, A. R., Bergametti, G., Brooks, N., Cao, J. J., Boyd, P. W., Duce, R. A., Hunter, K. A., Kawahata, H., Kubilay, N., laRoche, J., Liss, P. S., Mahowald, N., Prospero, J. M., Ridgwell, A., Tegen, I., and Torres, R.: Global iron connections between desert dust, ocean biogeochemistry, and climate, Science, 308, 67–71, 2005.

Measurements of dust deposition velocity

J. Zhang et al.

Title Page

Abstract	Introduction
Conclusions	References
Tables	Figures

|◀ | ▶|

| ◀ | ▶ |

| Back | Close |

Full Screen / Esc

Printer-friendly Version

Interactive Discussion

Liu, L. Y., Shai, P. J., Gao, S. Y., Zou, X. Y., Erdon, H., Yan, P., Li, X. Y., Ta, W. Q., Wang, W. Q., and Zhang, C. L.: Dustfall in China's western loess plateau as influenced by dust storm and haze events, Atmos. Environ., 38, 1699–1703, 2004.

Marticorena, B. and Bergametti, G.: Modeling the atmospheric dust cycle: 1. Design of a soil-derived dust emission scheme, J. Geophys. Res., 100, 16415–16430, 1995.

Nemitz, E., Gallagher, M. W., Duyzer, J. H., and Fowler, D.: Micrometeorological measurements of particle deposition velocities to moorland vegetation, Q. J. Roy. Meteor. Soc., 128, 2281–2300, 2002.

Ould-Dada, Z.: Dry deposition profile of small particles within a model spruce canopy, Sci. Total Environ., 286, 83–96, 2002.

Petroff, A., Mailliat, A., Amielh, M., and Anselmet, F.: Aerosol dry deposition on vegetative canopies. Part I: Review of present knowledge, Atmos. Environ., 42, 3625–3653, 2008.

Pérez, C., Nickovic, S., Pejanovic, G., Baldasano, J. M., and Özsoy, E.: Interactive dust-radiation modeling: a step to improve weather forecasts, J. Geophys. Res., 111, D16206, doi:10.1029/2005JD006717, 2006.

Pope III, C. A. and Dockery, D. W.: Epidemiology of particle effects, Air Pollution and Health, 31, 673–705, 1999.

Pryor, S. C., Larsen, S. E., Sørensen, L. L., Barthelmie, R. J., Grönholm, T., Kulmala, M., Launiainen, S., Rannik, Ü., and Vesala, T.: Particle fluxes over forests: analyses of flux methods and functional dependencies, J. Geophys. Res., 112, D07205, doi:10.1029/2006JD008066, 2007.

Pryor, S. C., Larsen, S. E., Sørensen, L. L., and Barthelmie, R. J.: Particle fluxes above forests: observations, methodological considerations and method comparisons, Environ. Pollut., 152, 667–678, 2008.

Reheis, M. C., Goodmacher, J. C., Harden, J. W., McFadden, L. D., Rockwell, T. K., Shroba, R. R., Sowers, J. M., and Taylor, E. M.: Quaternary soils and dust deposition in southern Nevada and California, Geol. Soc. Am. Bull., 107, 1003–1022, 1995.

Sehmel, G. A.: Particle diffusivities and deposition velocities over a horizontal smooth surface, J. Colloid Interf. Sci., 37, 891–906, 1971.

Seinfeld, J. H. and Pandis, S. N.: Atmospheric Chemistry and Physics: from Air Pollution to Climate Change, John Wiley, New York, 1998.

Shao, Y.: A model for mineral dust emission, J. Geophys. Res., 106, 20239–20254, 2001.

Title Page

Abstract | Introduction

Conclusions | References

Tables | Figures

|◀ | ▶|

◀ | ▶

Back | Close

Full Screen / Esc

Printer-friendly Version

Interactive Discussion

Shao, Y.: Simplification of a dust emission scheme and comparison with data, J. Geophys. Res., 109, D10202, doi:10.1029/2003JD004372, 2004.

Shao, Y.: Physics and Modelling of Wind Erosion, 2 edn., Springer, Berlin, 2008.

Shao, Y., McTainsh, G. H., Leys, J. F., and Raupach, M. R.: Efficiencies of sediment samplers for wind erosion measurement, Soil Research, 31, 519–532, 1993.

Shao, Y., Yang, Y., Wang, J. J., Song, Z. X., Leslie, L. M., Dong, C. H., Zhang, S. H., Lin, Z. H., Kanai, Y., Yabuki, S., and Chun, Y. S.: Real-time numerical prediction of northeast Asian dust storms using an integrated modeling system, J. Geophys. Res., 108, 4691, doi:10.1029/2003JD003667, 2003.

Slinn, S. A. and Slinn, W. G. N.: Predictions for particle deposition on natural waters, Atmos. Environ., 14, 1013–1016, 1980.

Slinn, W. G. N.: Predictions for particle deposition to vegetative canopies, Atmos. Environ., 16, 1785–1794, 1982.

Sokolik, I. N. and Toon, O. B.: Direct radiative forcing by anthropogenic airborne mineral aerosols, Nature, 381, 681–683, 1996.

Sow, M., Goossens, D., and Rajot, J. L.: Calibration of the MDCO dust collector and of four versions of the inverted frisbee dust deposition sampler, Geomorphology, 82, 360–375, 2006.

Tanaka, T. Y. and Chiba, M.: A numerical study of the contributions of dust source regions to the global dust budget, Global Planet. Change, 52, 88–104, 2006.

Textor, C., Schulz, M., Guibert, S., Kinne, S., Balkanski, Y., Bauer, S., Berntsen, T., Berglen, T., Boucher, O., Chin, M., Dentener, F., Diehl, T., Easter, R., Feichter, H., Fillmore, D., Ghan, S., Ginoux, P., Gong, S., Grini, A., Hendricks, J., Horowitz, L., Huang, P., Isaksen, I., Iversen, I., Kloster, S., Koch, D., Kirkevåg, A., Kristjansson, J. E., Krol, M., Lauer, A., Lamarque, J. F., Liu, X., Montanaro, V., Myhre, G., Penner, J., Pitari, G., Reddy, S., Seland, Ø., Stier, P., Takemura, T., and Tie, X.: Analysis and quantification of the diversities of aerosol life cycles within AeroCom, Atmos. Chem. Phys., 6, 1777–1813, doi:10.5194/acp-6-1777-2006, 2006.

Textor, C., Schulz, M., Guibert, S., Kinne, S., Balkanski, Y., Bauer, S., Berntsen, T., Berglen, T., Boucher, O., Chin, M., Dentener, F., Diehl, T., Feichter, J., Fillmore, D., Ginoux, P., Gong, S., Grini, A., Hendricks, J., Horowitz, L., Huang, P., Isaksen, I. S. A., Iversen, T., Kloster, S., Koch, D., Kirkevåg, A., Kristjansson, J. E., Krol, M., Lauer, A., Lamarque, J. F., Liu, X., Montanaro, V., Myhre, G., Penner, J. E., Pitari, G., Reddy, M. S., Seland, Ø., Stier, P., Takemura, T., and Tie, X.: The effect of harmonized emissions on aerosol properties in global models – an

AeroCom experiment, Atmos. Chem. Phys., 7, 4489–4501, doi:10.5194/acp-7-4489-2007, 2007.

Uno, I., Harada, K., Satake, S., Hara, Y., and Wang, Z.: Meteorological characteristics and dust distribution of the Tarim Basin simulated by the nesting RAMS/CFORS dust model, J. Meteorol. Soc. Jpn., 83A, 219–239, 2005.

Uno, I., Wang, Z., Chiba, M., Chun, Y. S., Gong, S. L., Hara, Y., Jung, E., Lee, S. S., Liu, M., Mikami, M., Music, S., Nickovic, S., Satake, S., Shao, Y., Song, Z., Sugimoto, N., Tanaka, T., and Westphal, D. L.: Dust model intercomparison DMIP study over Asia: overview, J. Geophys. Res., 111, D12213, doi:10.1029/2005JD006575, 2006.

Wesely, M. L., Cook, D. R., and Hart, R. L.: Fluxes of gases and particles above a deciduous forest in wintertime, Bound.-Lay. Meteorol., 27, 237–255, 1983.

Wesely, M. L., Cook, D. R., Hart, R. L., and Speer, R. E.: Measurements and parameterization of particulate sulfur dry deposition over grass, J. Geophys. Res., 90, 2131–2143, 1985.

Zender, C. S., Bian, H., and Newman, D.: Mineral Dust Entrainment and Deposition (DEAD) model: description and 1990s dust climatology, J. Geophys. Res., 108, D14416, doi:10.1029/2002JD002775, 2003.

Discussion Paper | Discussion Paper | Discussion Paper | Discussion Paper |

ACPD

14, 9439–9474, 2014

Measurements of dust deposition velocity

J. Zhang et al.

Title Page

Abstract | Introduction

Conclusions | References

Tables | Figures

|◀ | ▶|

◀ | ▶

Back | Close

Full Screen / Esc

Printer-friendly Version

Interactive Discussion

Table B1. List of wind-tunnel experiments.

Surfaces	Fan speed and Repeat times			
	3000 rpm ($\sim 3\,\mathrm{m\,s^{-1}}$)	6000 rpm ($\sim 5\,\mathrm{m\,s^{-1}}$)	9000 rpm ($\sim 8\,\mathrm{m\,s^{-1}}$)	12 000 rpm ($\sim 11\,\mathrm{m\,s^{-1}}$)
Water	3	3	3	/
Sticky wood plane	3	/	3	3
Sand	3	3	4	/
Sandy loam	3	3	3	/
Gobi surface	3	3	3	/
Tree	3	3	/	3

Table B2. Dust deposition velocity for different particle sizes, wind speeds and surface conditions.

Particle Diameter (µm)	Deposition velocity $w_d(z)$ (mm s⁻¹) on wood plane ($z = 15$ mm, $z_d = 0$ mm)		
	u_* (m s⁻¹) 0.12 z_0 (mm) 0.08	0.40 0.03	0.54 0.03
1	*0.08 ± /	*0.09 ± /	*0.09 ± /
2.25	0.48 ± 7.16	*0.88 ± /	*1.42 ± 18.21
4	2.16 ± 13.15	3.92 ± 8.60	28.78 ± 3.42
7.5	3.52 ± 3.89	32.35 ± 11.45	55.02 ± 11.46
12.5	13.86 ± 3.96	33.24 ± 6.04	82.12 ± 13.65
17.5	24.13 ± 2.11	39.00 ± 5.37	78.20 ± 22.99
22.5	32.79 ± 2.01	74.90 ± 14.32	89.66 ± 6.20
27.5	53.35 ± 0.30	63.52 ± 5.42	94.86 ± 42.90
40	108.70 ± 0.24	163.72 ± 49.74	156.05 ± 4.04

Particle Diameter (µm)	Deposition velocity $w_d(z)$ (mm s⁻¹) on water surface ($z = 25$ mm, $z_d = 0$ mm)		
	u_* (m s⁻¹) 0.15 z_0 (mm) 0.30	0.37 0.31	0.57 0.31
1	20.07 ± 11.85	79.68 ± 75.35	68.65 ± 65.51
2.25	26.90 ± 9.86	54.45 ± 41.55	114.86 ± 106.63
4	21.57 ± 5.1	56.79 ± 33.14	101.05 ± 58.07
7.5	22.79 ± 4.21	44.00 ± 9.24	120.70 ± 50.24
12.5	33.36 ± 8.37	61.32 ± 23.54	97.50 ± 37.93
17.5	41.87 ± 5.47	79.59 ± 23.38	122.56 ± 55.14
22.5	54.77 ± 9.44	101.36 ± 22.5	153.46 ± 68.54
27.5	68.17 ± 8.35	115.21 ± 32.65	176.56 ± 62.62
40	128.48 ± 6.80	179.70 ± 31.94	240.83 ± 46.5

Particle Diameter (µm)	Deposition velocity $w_d(z)$ (mm s⁻¹) on sand surface ($z = 15$ mm, $z_d = 0$ mm)		
	u_* (m s⁻¹) 0.14 z_0 (mm) 0.15	0.32 0.14	0.49 0.13
1	*0.41 ± /	*0.54 ± /	*6.69 ± /
2.25	1.00 ± 1.06	6.92 ± 11.64	12.74 ± 11.64
4	2.95 ± 2.64	12.99 ± 1.76	*16.2127
7.5	6.72 ± 5.76	19.71 ± 4.65	24.37 ± 4.65
12.5	14.79 ± 1.22	23.29 ± 6	23.07 ± 6
17.5	23.65 ± 4.03	26.51 ± 6.01	50.17 ± 6.01
22.5	35.91 ± 3.39	55.56 ± 6.42	47.21 ± 6.42
27.5	51.33 ± 3.88	47.01 ± 21.35	96.34 ± 21.35
40	113.69 ± 4.3	121.97 ± 1.76	123.48 ± 1.76

Table B2. Continued.

Particle Diameter (μm)	Deposition velocity $w_d(z)$ (mm s^{-1}) on sandy loam surface ($z = 15$ mm, $z_d = 0$ mm)		
	u_* (m s^{-1}) 0.17	0.40	0.60
	z_0 (mm) 0.85	0.84	0.68
1	*4.86 ± /	8.21 ± 9.85	*20.12 ± /
2.25	*6.32 ± /	26.24 ± 2.35	37.34 ± 24.88
4	7.89 ± 0.97	35.71 ± 4.13	53.61 ± 5.47
7.5	12.05 ± 3.87	37.64 ± 13.89	64.41 ± 6.5
12.5	19.72 ± 2.93	48.20 ± 17.19	81.11 ± 15.57
17.5	30.34 ± 2.28	64.89 ± 20.73	103.56 ± 25.54
22.5	43.94 ± 4.36	67.40 ± 14.14	90.32 ± 0.03
27.5	57.92 ± 8.90	90.44 ± 8.21	102.61 ± 22.95
40	119.43 ± 0.94	145.73 ± 7.76	178.70 ± 5.40

Particle Diameter (μm)	Deposition velocity $w_d(z)$ (mm s^{-1}) on Gobi surface ($z = 15$ mm, $z_d = 0$ mm)		
	u_* (m s^{-1}) 0.19	0.43	0.67
	z_0 (mm) 1.58	1.09	1.05
1	5.86 ± 4.86	*37.28 ± /	/
2.25	10.01 ± 8.91	63.72 ± 46.8	/
4	10.31 ± 6.14	51.48 ± 35.72	/
7.5	*16.40 ± /	16.46 ± 51.58	/
12.5	*25.62 ± /	47.73 ± 20.9	/
17.5	34.79 ± 3.39	42.39 ± 0.32	/
22.5	61.10 ± 16.08	132.03 ± 84.78	/
27.5	73.61 ± 21.95	69.00 ± 66.8	/
40	114.19 ± 1.91	142.40 ± 6.35	/

Particle Diameter (μm)	Deposition velocity $w_d(z)$ (mm s^{-1}) on tree surface ($z = 250$ mm, $z_d = 200$ mm)		
	u_* (m s^{-1}) 0.24	0.50	1.06
	z_0 (mm) 5.93	2.88	2.10
1	2.38 ± 19.27	9.24 ± 39.35	*48.04 ± /
2.25	6.13 ± 16.08	15.79 ± 40.74	*67.59 ± /
4	*7.76 ± /	42.96 ± 30.58	79.39 ± 119.73
7.5	9.13 ± 13.52	36.03 ± 42.69	*119.79 ± /
12.5	*20.14 ± /	*35.28 ± /	137.55 ± 116.91
17.5	41.25 ± 44.56	54.68 ± 130.33	203.97 ± 76.49
22.5	*43.71 ± /	37.81 ± 114.76	246.57 ± 138.4
27.5	*59.87 ± /	42.91 ± 74.84	403.57 ± 221.76
40	107.28 ± 14.26	130.26 ± 113.86	328.59 ± 154.32

* Estimated from the dust profile (polynomials) fitted to the experimental data.
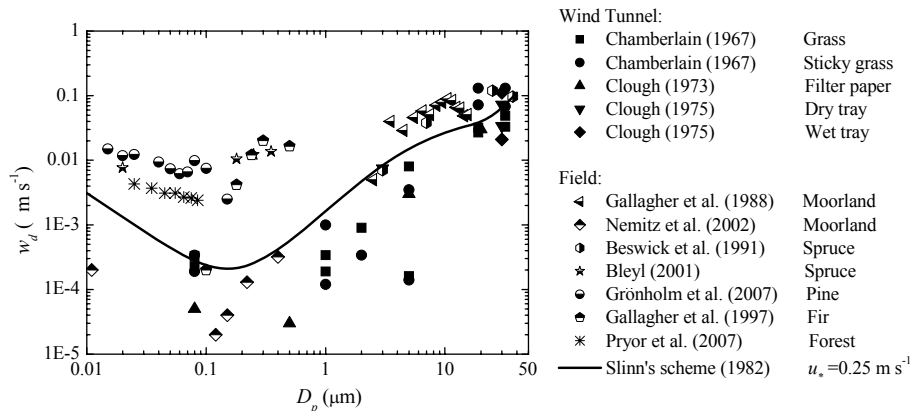
Fig. 1. Some existing measurements of deposition velocities against particle size for different surfaces.
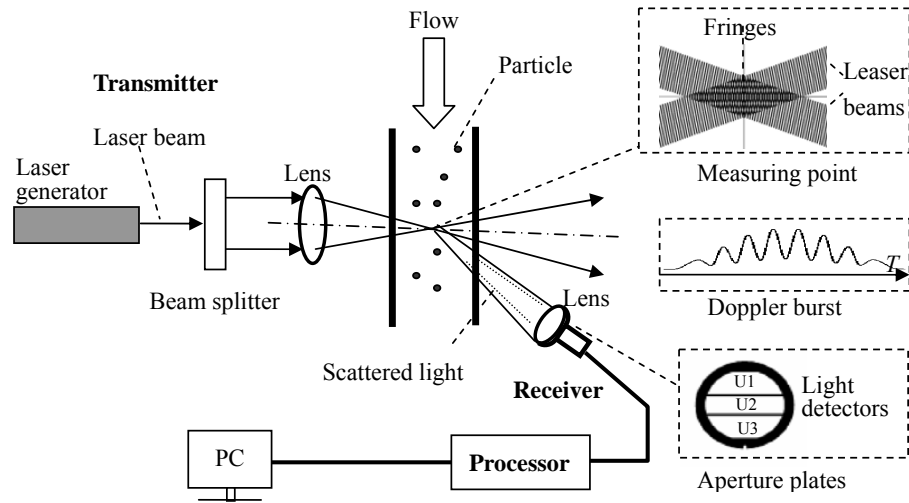
Fig. 2. Basic structure of the PDA. The velocities and sizes of the particles passing through the measuring point are obtained by analyzing the light scattered by the particles.
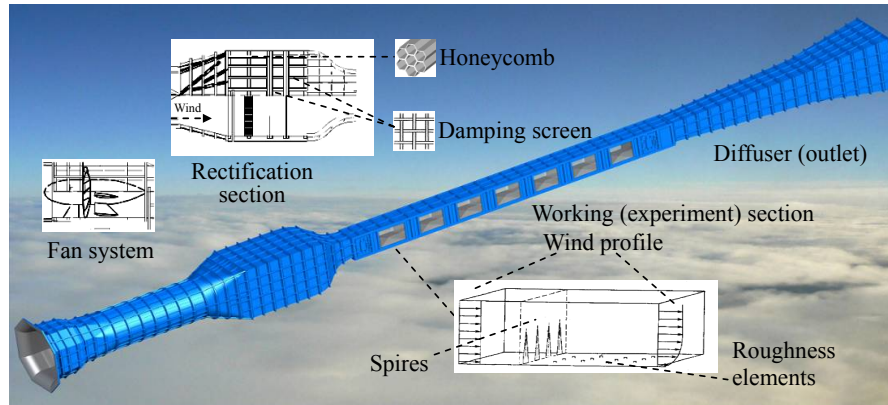
Fig. 3. A sketch of the Lanzhou University wind tunnel.
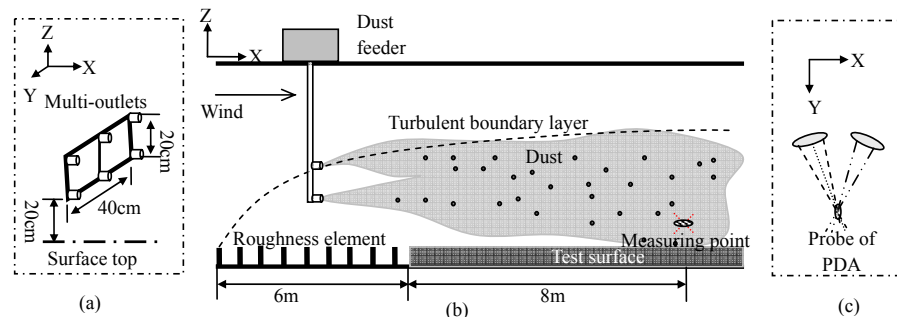
Fig. 4. Configuration of the wind-tunnel experiment. **(a)** Dust feeding outlets; **(b)** working section; the roughness elements fixed at the front of the working section generate a deep (at least 0.4 m) turbulent boundary layer. Downstream of the roughness-element section is the test surface. Dust feeder is placed at the beginning of the working section and injects dust (SiO_2) into the tunnel through a tubular manifold. The measuring point is located near the end of the working section; **(c)** probe of the PDA with laser beams intersecting at the measuring point.
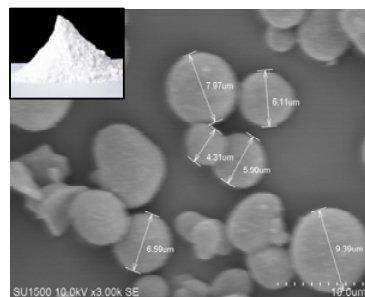
(a)
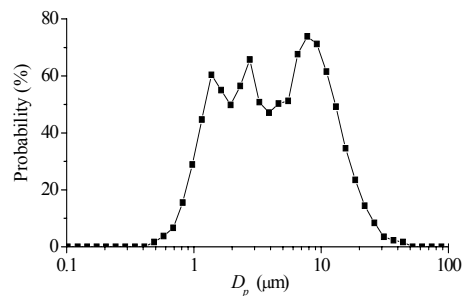
(b)

Fig. 5. SiO$_2$ powder used as dust for the wind-tunnel experiment. **(a)** Powder appearance (top left corner) and microscopic picture (measured by Scanning Electron Microscope, SU1500); **(b)** probabilistic distribution of particle size (measured by Particle Size Analyzer, S3500).
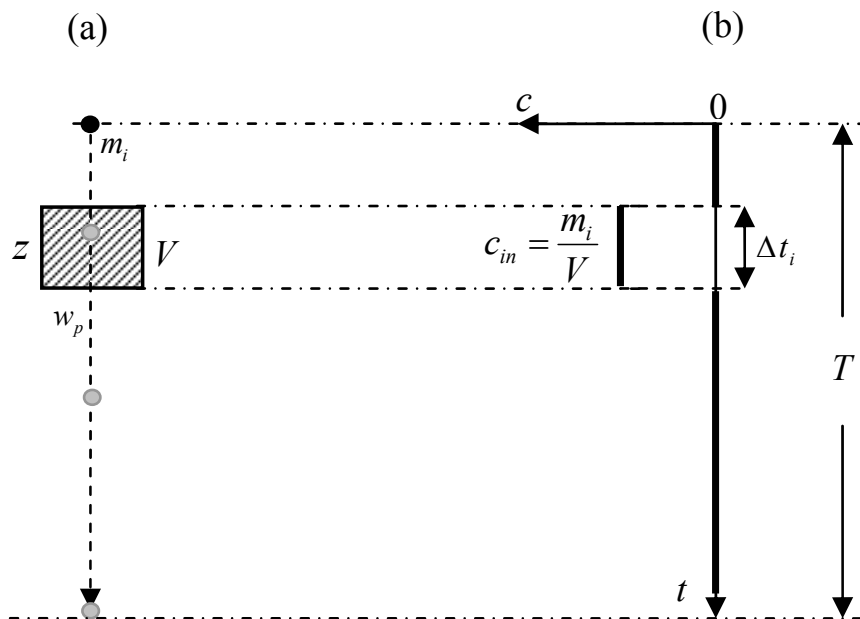
Fig. 6. Illustration of one particle's contribution to dust concentration and flux. **(a)** A dust particle (dot) passes through the sampling area (shaded); **(b)** dust concentration corresponding to the situation shown in **(a)**.

Title Page

Abstract | Introduction

Conclusions | References

Tables | Figures

|◀ | ▶|

◀ | ▶

Back | Close

Full Screen / Esc

Printer-friendly Version

Interactive Discussion
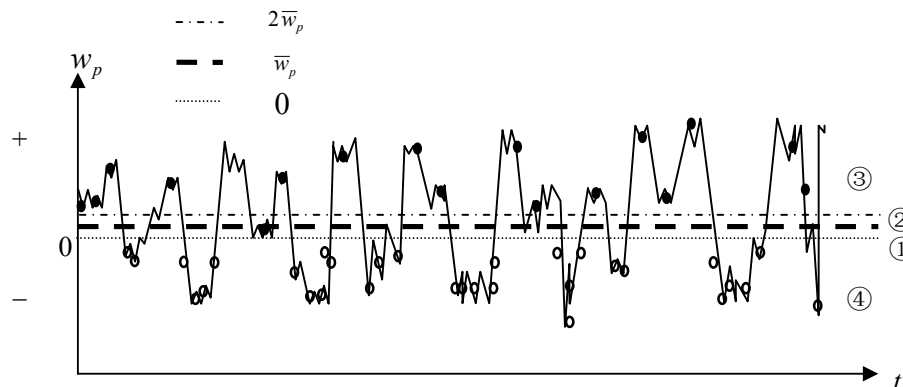
Fig. 7. Illustration of the PDA data of particle velocity. Solid and open dots represent positive and negative w_p measured by the PDA, respectively, and the solid line $w_a + w_t$. As an example, suppose $\overline{w}_p > 0$, the full dataset is divided into four parts: (1) $0 < w_p < \overline{w}_p$; (2) $\overline{w}_p < w_p < 2\overline{w}_p$; (3) $w_p > 2\overline{w}_p$; and (4) $\overline{w}_p < 0$.

Fig. 8. Examples of the test surfaces of **(a)** water, and **(b)** trees.
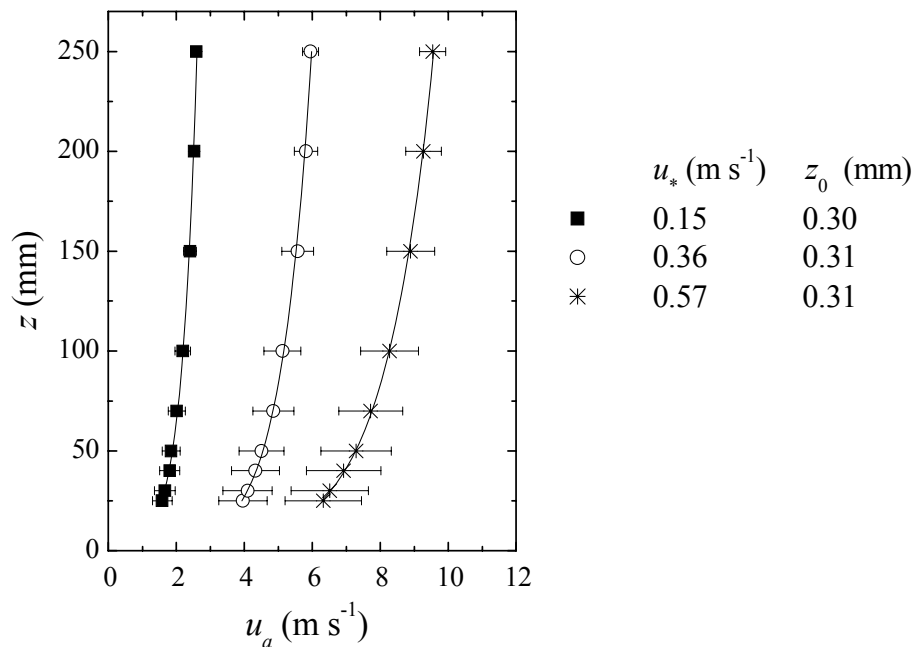
Fig. 9. Wind profiles measured over the water surface for three experiments with the fan speed set to 3000, 9000 and 12 000 rpm. The symbols are the mean wind speeds, and the error bars show the standard deviations. The curves are the logarithmic profiles fitted to the data.
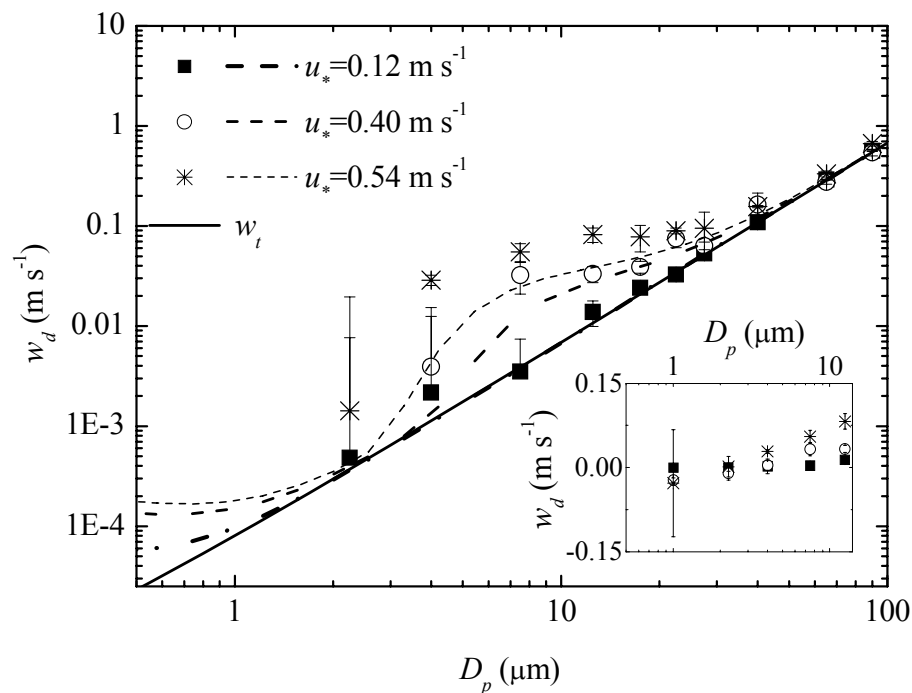
Fig. 10. Deposition velocity against particle size under different wind conditions over the wood surface. The symbols are averaged w_d and the error bars represent the variability of the three runs. The curves are the results predicted with the SS80 scheme. The height of the measuring point is 15 mm above the wood surface. w_d for small particles (1–12.5 µm) have been inserted in the lower right corner to display the possible negative deposition velocities which impossibly appear in logarithmic coordinate system.

Title Page

Abstract | Introduction

Conclusions | References

Tables | Figures

|◄ | ►|

◄ | ►

Back | Close

Full Screen / Esc

Printer-friendly Version

Interactive Discussion
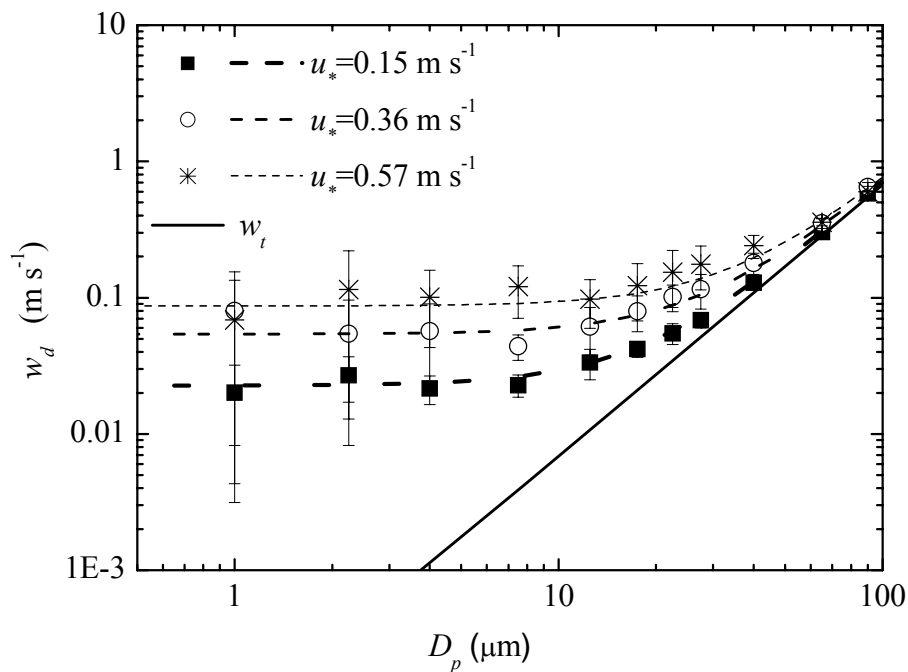
Fig. 11. As Fig. 10, but is for the water surface. The curves are the results predicted with the SS80 scheme by setting the laminar layer resistance $1/w_D$ to zero. The height of the measuring point is 25 mm above the water surface.
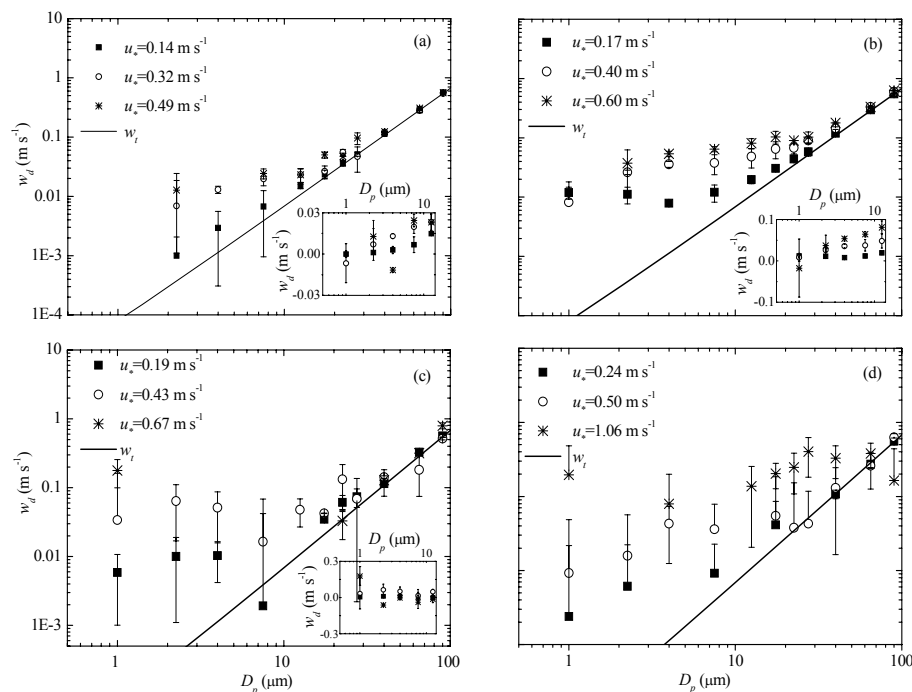
Fig. 12. As Fig. 10, but are for **(a)** sand, **(b)** sandy loam, **(c)** Gobi and **(d)** tree surface. For the tree surface, the measurement height is $z = 250$ mm.
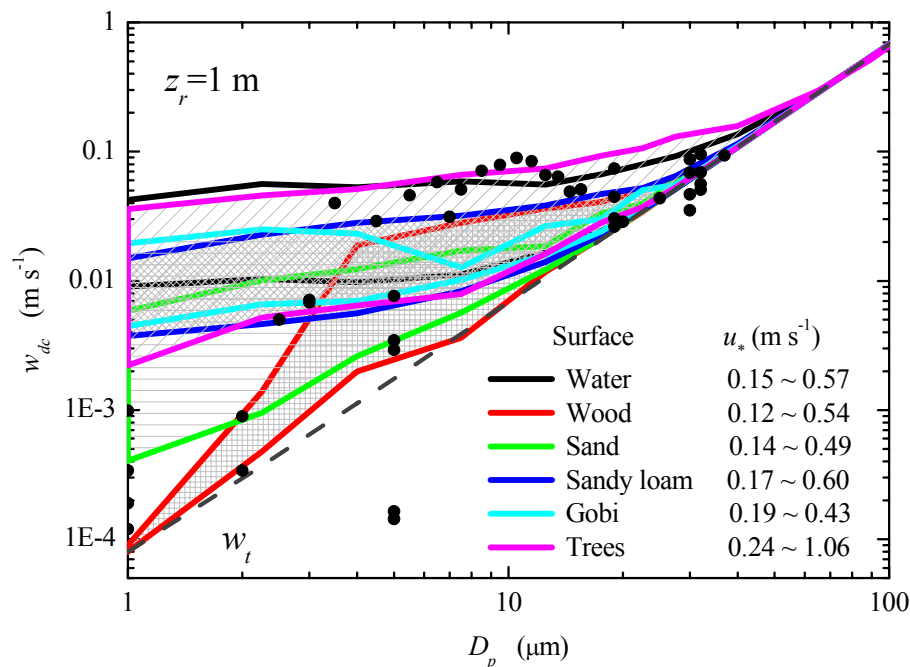
Fig. 13. Comparison between the results of our and other existing experiments. The lines and the shaded areas represent the range of dust deposition velocity over different surfaces, extracted from our dataset. The dots are the results of the existing works shown in Fig. 1. All measurements are corrected to the same reference height (1 m).

z_r — Mean wind at reference height

Constant Flux layer: Turbulent transfer and settling

δ — Deposition layer: Impaction, Brownian diffusion, settling and particle size growth.

Water surface
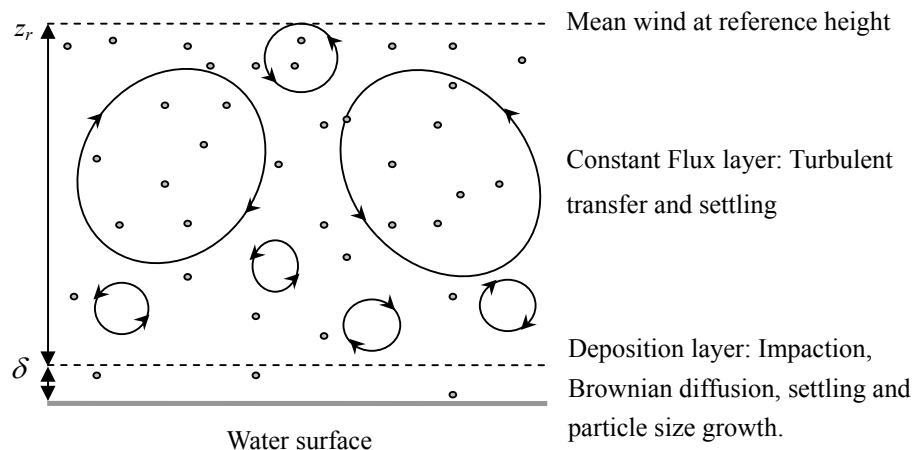
Fig. A1. A schematic illustration of the two-layer model for dust deposition to a smooth surface.